

Characterization of different high amylose starch granules. Part I: Multi-scale structures and relationships to thermal properties

Yu Tian^a, Xingxun Liu^b, Jacob Judas Kain Kirkensgaard^{c,d}, Bekzod Khakimov^c, Kasper Enemark-Rasmussen^e, Kim Henrik Hebelstrup^{f,g}, Andreas Blennow^{a,**}, Yuyue Zhong^{a,*}

^a Department of Plant and Environmental Sciences, University of Copenhagen, 1871, Frederiksberg C, Denmark

^b Lab of Food Soft Matter Structure and Advanced Manufacturing, College of Food Science and Engineering/Collaborative Innovation Center for Modern Grain Circulation and Safety/, Nanjing University of Finance and Economics, Nanjing, 210023, China

^c Department of Food Science, University of Copenhagen, DK-1958, Frederiksberg C, Denmark

^d Niels Bohr Institute, University of Copenhagen, DK-2100, Copenhagen Ø, Denmark

^e Department of Chemistry, Technical University of Denmark, DK-2800, Kemitorvet, Building 207 Kgs, Lyngby, Denmark

^f Department of Agroecology, Section for Crop Genetics and Biotechnology, Aarhus University, 4200, Flakkebjerg, Denmark

^g PlantCarb ApS, Vedbæk, Denmark

ARTICLE INFO

Keywords:

High amylose
Amylose fine structure
Helical structure
Starch crystallinity
Lamellar structure
Degree of branching

ABSTRACT

The multi-scale structure and thermal properties of eight widely different types of high-amylose starches (HASs) having amylose contents (AC) in the range of 34.4%–97.3% originating from maize, wheat, barley, and potato were analyzed to unveil possible relationships among different levels of structures and thermal properties. The starches were found to cluster in four groups: (I) two HASs from maize, Gelose50 and Gelose80, with high gelatinization enthalpy (ΔH) and low onset (T_0) and peak (T_p) gelatinization temperatures, (II) two HASs from potato and wheat, with medium and high ΔH and extremely low T_0 and T_p , (III) two HASs from maize, NAFU50 and NAFU60, with medium ΔH and medium T_0 and T_p , (IV) two HASs from maize and barley, Hylon VII and AOBs, with low ΔH but high T_0 and T_p . The degree of molecular branching and the extent of the granule V-type crystalline polymorph were the critical factors determining their thermal properties, while botanical source and AC were not found important. HASs from wheat and barley showed relatively low lamellar and crystalline order, which was related to high content of amylopectin or AM-like chains with degree of polymerization (DP) 6–12 and long amylose chains, both of which can contribute to prevent the formation of double helices. Our data pinpoint the importance of amylopectin short chains, amylose long chains, and degree of branching on HAS starch granule structural order and thermal stability, which are potentially useful in boosting the development of HAS-based products and be beneficial for developing new HAS crops.

1. Introduction

Starch is one of the most important sources of human dietary energy, and is also a common raw material in non-food industries, such as paper, drug delivery, adhesive, and binder (Zhong, Tai, et al., 2022). Native starch granules display quite complex, conserved, hierarchical structures with discrete levels of organization: molecular structure (0.1 nm), crystalline and amorphous lamellar structure (8–11 nm), alternating amorphous and semi-crystalline growth rings and blocklets (0.1 μm) and granular structure (1–100 μm) (Bertoft, 2017; Tian et al., 2023). Highly branched amylopectin (AP) molecules and mainly linear amylose (AM)

molecules are the main contributors of these multi-scale structures.

Gelatinization is a pivotal process in both food and non-food applications of starches. Differential Scanning Calorimetry (DSC) is widely recognized as a tool for discerning the parameters associated with the transition from order to disorder in semi-crystalline starch granules during their heating in an excess aqueous environment (Wootton & Bamunuarachchi, 1979). Typically, it has been suggested that, as the AM content in starch rises, so does the gelatinization temperature (C. Li, Dhital, Gilbert, & Gidley, 2020). Several potential mechanisms have been proposed to elucidate the thermal resistance of high amylose starch (HAS) (Zhong, Tai, et al., 2022): (1) The enhanced AM content of HAS, which is thermally more stable than typical starch types, is situated in

* Corresponding author.

** Corresponding author.

E-mail addresses: abl@plen.ku.dk (A. Blennow), yuyuezhong93@163.com (Y. Zhong).

<https://doi.org/10.1016/j.foodhyd.2023.109286>

Received 5 July 2023; Received in revised form 29 August 2023; Accepted 11 September 2023

Available online 15 September 2023

0268-005X/© 2023 Elsevier Ltd. All rights reserved.

Abbreviations	
HAS	high amylose starch
AM	amylose
AP	amylopectin
SEC	size-exclusion chromatography
HPAEC-PAD	high-performance anion exchange chromatography-pulsed amperometric detection
WAXS	wide angle X-ray scattering
SAXS	small angle X-ray scattering
SEM	scanning electron microscopy
NMR	nuclear magnetic resonance
FTIR	Fourier transform infrared-attenuated total reflectance
DMSO	dimethyl sulfoxide
AAC	apparent amylose content analyzed by iodine complexation
RC _x	relative amount of fraction X
ACL:	Average chain length
ACL _x	ACLs (DP) of fraction X
β _{ami}	high value refers to shorter amylose chains in the ith region
h _{amx}	high value refers to high amount of amylose chains in the
	Xth region
Rh _{na-x} :	hydrodynamic radius of fraction X of native sample
fa	amylopectin chains with DP 6–12
fb ₁	amylopectin chains with DP 13–24
fb ₂	amylopectin chains with DP 25–36
fb ₃	amylopectin chains with DP > 36
Ap ₁	short amylopectin chains (DP 6–30) analyzed by SEC
Ap ₂	long amylopectin chains (DP 30–220) analyzed by SEC
Am	amylose chains (DP 220–10000) analyzed by SEC
DP	degree of polymerization
D	bragg lamellar repeat distance
d _a	thickness of amorphous lamellae
d _c	thickness of crystalline lamellae
d _{ac}	long period distance
W	the full width at half maximum (M) of peak in reciprocal space from the SAXS data fitting
T _o	gelatinization onset temperature
T _p :	gelatinization peak temperature
T _c	gelatinization conclusion temperature
ΔH	gelatinization enthalpy

the exterior layers (Kuakpetoon & Wang, 2007). (2) The presence of longer double helices in HAS, possibly formed by AM-AM, AM-lipid, and elongated AP chains, exhibit elevated melting temperatures (Cai, Zhao, Huang, Chen, & Wei, 2014). Furthermore, it is suggested that the longer double helices in HAS that protrude into the amorphous regions might offer stability to these areas, thereby elevating the onset of the melting temperature (H. Li, Gidley, & Dhital, 2019). (3) There is potential for AM to spontaneously establish new double helices and crystallites with AP, AM, and lipids throughout the gelatinization phase (Cai, et al., 2014). These dynamic changes contribute to the stabilization of starch granules. However, for various HAS types that all display a relatively high AM content, the specific features, apart from AM, that influence their distinct thermal stability remain unclear due to the limited comparative structural data on different HAS.

For decades, a series of HAS mutants have been developed from various crops, e.g., maize, wheat, and potato, etc., by traditional and molecular breeding techniques (Blennow, et al., 2005; Zhong, Qu et al., 2022). However, HAS genotypes with same AM content but different genetic backgrounds, even from the same crop species, have been demonstrated to have very different structures and physicochemical properties. It has been shown that (I) three types of starch branching enzyme IIB (SBEIIB) - deficient HAS genotypes from same botanical source (maize), NAFU50, Gelose 50, and HylonVII exhibited differences in granular size and resistant starch content (R. Li et al., 2023) and (II) HASs from wheat (RS101 and RS100) had more flexible chains than HASs from maize (Gelose 50 and Gelose 80) (H. Li, Dhital, Flanagan, et al., 2020). This implies that HASs are exceptionally diverse. Unfortunately, no comprehensive and systematic data of HASs from different genetic backgrounds and different crops is available, which limits efficient and predictive breeding and application of HAS crops. Such data are also important to relate to how the starch molecular structure is molecularly represented, which is to date an ongoing discussion. Hence, the recent so called building block backbone (Bertoft, 2017) and the traditional tree-like cluster models are up to discussion. To this end, the backbone model, describing the configuration of shorter and mainly double-helical chains (Bertoft, 2017), sparsely and mainly radially extend from longer and tangentially organized backbone chains providing flexibility found in HAS type starches.

Hence, in this study, eight types of HASs from four types of botanical source, including five maize types, NAFU50 (Zhong, Liu, Qu, Li, et al., 2020), NAFU60 (Zhong, Liu, Qu, Li, et al., 2020), Gelose 50 (H. Li,

Dhital, Flanagan, et al., 2020), Gelose 80 (H. Li, Dhital, Flanagan, et al., 2020), and Hylon VII (Agama-Acevedo, Pacheco-Vargas, Bello-Pérez, & Alvarez-Ramirez, 2018; R. Li et al., 2023), the AM-only starch from barley (AOBS) (Carciofi, et al., 2012), HAS from wheat (HAWs), and HAS from potato (HAPS) (Blennow, et al., 2005), were selected to compare the multistructural and gelatinization properties of different HASs. The primary goal of this study is to offer a comprehensive multi-structural analysis of various HAS, particularly focusing on their gelatinization properties, to lay a foundation to better understand their potential applications and nutritional benefits in food.

2. Material and methods

2.1. Starch and enzyme sources

Three types of high amylose maize starches, NAFU50, NAFU60 (Zhong, Liu, Qu, Li, et al., 2020), and Hylon VII, and high amylose wheat starch (HAWs) were provided by Maize Genetic Breeding Laboratory, Northwest A&F University, Yangling, China. The other two types of high amylose maize starches, Gelose 50 and Gelose 80 were from Penford Australia Ltd., NSW, Australia. Amylose-only starch from barley (AOBS) and high amylose potato starch were prepared as described (Blennow, et al., 2005; Carciofi et al., 2012). The apparent AM content (AAC) and background information of these starches are shown in Table 1 and Table S1. Isoamylase (*E-ISAMY*, 200 U/mL) was purchased from Megazyme (Ireland). Other chemical reagents were from Sigma-Aldrich (St. Louis, MO, USA).

2.2. Apparent amylose content (AAC)

Five mg of starch powder (dry basis) was dissolved in 0.75 mL of 4 M NaOH overnight with vigorous stirring, and 2.25 mL of MilliQ water added to adjust the concentration of NaOH to 1 M. Finally, 10 μL sample was mixed with 200 μL 10-fold diluted Lugol solution (pH = 2), the absorbance measured at 550 and 620 nm and AAC calculated from standards (Carciofi, et al., 2012).

2.3. Size-exclusion chromatography (SEC)

A size exclusion chromatography-triple detector array SEC-TDA (Viscotek, Malvern, UK) instrument was used to analyze the chain

Table 1

Relative contents (RC) and average chain lengths (ACL) of debranched AP and AM fractions as deduced from SEC data.

Sample	AAC %	RC _{de- Ap1} (%)	RC _{de- Ap2} (%)	RC _{de- Am} (%)	ACL de-Ap1	ACL de-Ap2	ACL de-Am	β_{am1} × 10 ⁻³	h_{am1} × 10 ⁻¹	β_{am2} × 10 ⁻³	h_{am2} × 10 ⁻¹	β_{am3} × 10 ⁻⁴	h_{am3} × 10 ⁻¹	Rh _{na- AP} (nm)	Rh _{na- AM} (nm)	RC _{na- AP} (%)	RC _{na- AM} (%)
NAFU50	51.6 ± 0.8 ^e	26.1 ± 0.2 ^c	34.3 ± 0.2 ^{cd}	39.6 ± 0.4 ^c	14.0 ± 0.0 ^{ab}	73.5 ± 0.2 ^d	1063 ± 1 ^{cd}	6.9 ± 0.5 ^b	1.9 ± 0.1 ^d	2.0 ± 0.1 ^{ab}	3.5 ± 0.1 ^d	5.6 ± 0.1 ^{abc}	2.8 ± 0.1 ^c	118.2 ± 1.1 ^b	7.7 ± 0.0 ^{de}	24.6 ± 0.3 ^c	75.4 ± 0.3 ^c
NAFU60	61.0 ± 2.1 ^d	23.6 ± 1.1 ^c	34.9 ± 0.5 ^{bc}	41.5 ± 0.6 ^c	13.9 ± 0.2 ^{ab}	76.1 ± 0.8 ^c	869 ± 6 ^f	7.1 ± 0.5 ^b	2.6 ± 0.2 ^{bc}	2.1 ± 0.3 ^{ab}	4.7 ± 0.0 ^{bc}	6.8 ± 1.2 ^a	2.3 ± 0.4 ^{cd}	114.2 ± 2.1 ^{bc}	7.3 ± 0.1 ^e	20.8 ± 0.4 ^d	79.2 ± 0.4 ^d
Gelose 50	40.7 ± 1.8 ^f	33.0 ± 1.4 ^b	33.2 ± 0.9 ^d	33.7 ± 0.5 ^d	13.3 ± 0.7 ^{ab}	70.2 ± 0.6 ^e	945 ± 17 ^e	6.0 ± 0.3 ^b	2.1 ± 0.2 ^{cd}	1.8 ± 0.1 ^{ab}	3.0 ± 0.2 ^d	5.7 ± 0.1 ^{abc}	1.7 ± 0.0 ^d	113.4 ± 0.3 ^{bc}	8.5 ± 0.1 ^d	31.5 ± 0.1 ^b	68.5 ± 0.1 ^f
Gelose 80	59.0 ± 0.4 ^d	24.3 ± 0.4 ^c	35.8 ± 0.3 ^b	39.9 ± 0.1 ^c	14.0 ± 0.2 ^{ab}	76.9 ± 0.1 ^c	881 ± 4 ^f	7.4 ± 0.3 ^b	3.1 ± 0.2 ^{ab}	2.1 ± 0.1 ^{ab}	4.1 ± 0.1 ^c	6.1 ± 0.2 ^{ab}	2.2 ± 0.1 ^d	111.8 ± 0.6 ^{bc}	7.7 ± 0.5 ^d	17.2 ± 1.8 ^e	82.8 ± 1.8 ^c
Hylon VII	72.3 ± 1.2 ^b	16.6 ± 1.3 ^d	33.9 ± 0.2 ^{cd}	49.6 ± 1.1 ^b	14.5 ± 0.8 ^a	80.8 ± 1.0 ^b	1030 ± 11 ^d	6.5 ± 0.4 ^b	3.3 ± 0.2 ^a	1.9 ± 0.1 ^{ab}	4.8 ± 0.4 ^b	5.1 ± 0.0 ^{bc}	3.8 ± 0.2 ^b	100.0 ± 5.1 ^d	7.4 ± 0.0 ^e	8.9 ± 0.8 ^g	91.1 ± 0.8 ^a
AOBS	97.3 ± 2.0 ^a	6.9 ± 0.7 ^e	18.7 ± 0.1 ^f	74.3 ± 0.7 ^a	14.9 ± 1.1 ^a	89.9 ± 1.7 ^a	1599 ± 12 ^a	3.7 ± 0.4 ^c	2.9 ± 0.0 ^{ab}	0.9 ± 0.1 ^c	5.6 ± 0.2 ^a	5.4 ± 0.1 ^a	5.4 ± 0.1 ^a	90.5 ± 2.5 ^c	11.5 ± 0.2 ^b	12.0 ± 21.0 ^f	88.0 ± 0.5 ^b
HAWS	67.2 ± 0.3 ^c	26.4 ± 0.5 ^c	25.1 ± 0.1 ^e	48.5 ± 0.7 ^b	12.2 ± 0.5 ^b	73.1 ± 0.0 ^d	1104 ± 4 ^c	6.5 ± 0.5 ^b	2.8 ± 0.1 ^{ab}	1.7 ± 0.0 ^b	5.7 ± 0.2 ^a	5.7 ± 0.1 ^{abc}	4.2 ± 0.1 ^b	108.2 ± 2.5 ^c	9.7 ± 0.1 ^c	21.0 ± 0.5 ^d	79.0 ± 0.5 ^d
HAPS	34.4 ± 1.0 ^g	37.4 ± 0.3 ^a	40.4 ± 0.1 ^a	22.2 ± 0.4 ^e	14.3 ± 0.1 ^a	68.0 ± 0.0 ^c	1385 ± 15 ^b	10.5 ± 1.5 ^a	0.7 ± 0.1 ^e	2.2 ± 0.1 ^a	1.1 ± 0.0 ^e	4.2 ± 0.1 ^c	1.7 ± 0.0 ^d	128.2 ± 3.3 ^a	13.9 ± 0.5 ^a	49.3 ± 0.8 ^a	50.7 ± 0.8 ^g

All data are means ± standard deviation (n = 2). Values with different letters in the same column are significantly different at $p < 0.05$.

AAC: apparent amylose content determined by iodine method; RC_{de-X}: relative amount of fraction X of debranched sample; RC_{na-X}: relative amount of fraction X of native sample; ACL_{de-X}: the average chain length (DP) of the fraction X of debranched sample; Rh_{na-X}: hydrodynamic radius of fraction X of native sample. β_{amX} : higher value means shorter chains in the *i*th region; h_{amX} : higher value means higher amount of chains in the *X*th region. Region 1: low DP region of amylose. Region 2: intermediate DP region of amylose. Region 3: high DP region of amylose.

length distributions (CLDs) of starches after isoamylase-assisted debranching. The instrument was equipped with a GRAM precolumn and GRAM1000 (Polymer Standard Services, Mainz, Germany) connected to TDA302 for detection array. The differential refractive index (DRI) signals were recorded using a refractive index detector (PN3140, PostNova Analytics, Landsberg, Germany), and the data analyzed using PSS WinGPC Unity software (Polymer Standard Services, Mainz, Germany).

The size distributions of whole starch molecules and starch chains were analyzed as described previously (Hongyan Li, Prakash, Nicholson, Fitzgerald, & Gilbert, 2016) with minor modifications. For analysis of the native starch, samples (5 mg) were dissolved in 1 mL DMSO/LiBr (0.5% w/w, Avantor, US) at 80 °C overnight at 300 rpm mixing and centrifuged at 20,000g for 5 min. The supernatant was injected onto the SEC-TDA system. Elution was performed using DMSO/LiBr at a flow rate of 0.5 mL/min and a column temperature of 65 °C. Isoamylase debranched samples were prepared by heating starch dispersion in screwed tubes with DMSO/LiBr (5 mg/mL) at 80 °C for 3h, the gelatinized starch was collected after centrifugation at 4000g for 10 min with absolute ethanol and allowed to dry in a fume hood at ambient temperature. Isoamylase (0.8 U) and 1 mL sodium acetate buffer (0.01M, pH 4.0) were added and the mixture incubated at 40 °C for 3 h 5 mg/mL of the freeze dried debranched samples dissolved in DMSO/LiBr were prepared before injecting onto the SEC-TDA system.

The CLDs of amylose chains were fitted to an AM biosynthesis model developed recently (Fig. S1A) (Nada, Zou, Li, & Gilbert, 2017). The length of chains, and the amount of chains in each fitting region are represented by the parameters of β_{amX} and h_{amX} (X = 1–3); e.g. the higher the β_{amX} value, the shorter the chain, and the higher the h_{amX} value, the higher the amount of chains in the region X (region 1 is the low degree of polymerization (DP) region of AM, region 2 is intermediate DP region of AM and region 3 is high DP region of AM).

2.4. High-performance anion exchange chromatography-pulsed amperometric detection (HPAEC-PAD)

Isoamylase enzymatic debranching was performed as described in section 2.3 and the debranched starch (40 µL, 5 mg/mL) was injected onto a CarboPac PA-200 column attached to an HPAEC-PAD (Dionex, Sunnyvale, CA, USA) system. Columns were pre-washed with 100 mM NaOH at 0.4 mL/min for 20 min. The elution process made use of three solutions: MilliQ water (eluent A), 1 M NaOH (eluent B), and 1 M NaOH enriched with 25 mM NaAc (eluent C). The elution gradient functioned at a rate of 0.4 mL/min and proceeded in the following manner: an initial phase of 0–5 min (with 15% of eluent A and 85% of eluent C), followed by 5–130 min (where eluent B increased linearly to 40% and eluent C dropped linearly to 45%), 130–135 min (with 80% eluent A and 20% eluent C), and lastly from 135 to 145 min (reverting to the original eluent mixture). Peak integration and detector response were performed as described (Blennow, Bay-Smidt, Wischmann, Olsen, & Møller, 1998).

2.5. Solution state proton (¹H) nuclear magnetic resonance (NMR) spectroscopy

A 600 MHz NMR spectrometer (Bruker Avance III, Bruker Biospin, Rheinstetten, Germany) was used to obtain one-dimensional ¹H NMR spectra, following the previously described procedure (Zhong, Herburger, et al., 2021). The starch samples (5 mg/mL) were gelatinized in DMSO-d₆ (methyl sulfoxide-d₆) containing 1 mg/mL trimethylsilyl propanoic acid (TSP), followed by lyophilization and re-dissolution in TSP/DMSO-d₆ (1 mL) at 90 °C for 1 h prior to analysis. Areas of signals representing anomeric protons (δ 5.35–5.45 α -1,4 and δ 4.95–5.00 α -1,6) were integrated to calculate the degree of glucan branching. SigMa software (Khakimov, Mobaraki, Trimigno, Aru, & Engelsen, 2020) was used to detect and calculate the signal areas.

2.6. Solid state ^{13}C nuclear magnetic resonance (NMR) spectroscopy

Solid-state ^{13}C NMR analysis was performed using a ^{13}C frequency of 75.46 MHz on a Bruker MSL-300 spectrometer as described (Tan, Flanagan, Halley, Whittaker, & Gidley, 2007). To prepare amorphous standard samples, starch suspensions (1% w/v in MilliQ water) (waxy maize, waxy wheat, waxy barley, and waxy potato) were gelatinized at 100 °C for 30 min. Approximately 300 mg starch was packed in a 4-mm diameter rotor and the rotor was spun at 5–6 kHz at the magic angle (54.7°). A 90° pulse width was 5 μs and a contact time of 1 ms was used for all starch samples with a recycle delay of 5 s. At least 2400 scans were accumulated for each spectrum with spectral width of 38 kHz, with an acquisition time of 3 ms. The relative content of the single helix (102–103 ppm), the double helix (99–101 ppm) and the amorphous regions were calculated as described (Tan, et al., 2007).

2.7. Wide angle X-ray scattering (WAXS)

Starch powders were conditioned with saturated KCl atmosphere for 72 h in a humidity chamber with a relative humidity of 90%, and data collected with a SAXSLab instrument (Xenocs Nano-inXider, Copenhagen, Denmark). The radial average intensities I , given as a function of the scattering angle 2θ in the range of 5–30°, were recorded at 40 mA current, 40 kV voltage and 0.1542 nm wavelength Cu K α radiation. Relative crystallinity was calculated using the PeakFit software (Version 4.12 Syntat Software, Inc., San Jose, CA, USA) and the amorphous background scattering and relative crystallinity were calculated as follow:

$$\text{Relative crystallinity (\%)} = \frac{\text{Peak areas}}{\text{Total area}}$$

2.8. Small angle X-ray scattering (SAXS)

The lamellar structure of starch granule suspensions (starch: water = 1:3) were analyzed using a Nano-InXider instrument (Xenocs, Grenoble) equipped with a 100 XL + microfocus sealed X-ray tube (Rigaku, The Woodlands Texas, USA) providing Cu-K α radiation with wavelength $\text{LAMBDA} = 1.54 \text{ \AA}$ and a 2D Pilatus detector (Dectris Ltd., Baden, Switzerland). Samples were measured for 15 min in quartz capillary tubes with 1.5 mm diameter. The air and water scattering were subtracted from the original SAXS data. Two different methods including normalized 1D correlation function and SAXS scattering curve fitting were used to analyze the SAXS data. A normalized 1D correlation function $\gamma_1(r)$ was used to obtain the thickness of crystalline (dc) and amorphous (da) lamellae (Kuang, et al., 2017).

$$\gamma_1(r) = \frac{\int_0^\infty I(q) q^2 \cos(qr) dq}{Q}$$

$$Q = \int_0^\infty I(q) q^2 dq$$

where $I(q)$ is the scattering intensity, q is the scattering vector defined as $q = 4\pi \sin\theta / \lambda$ (2θ is the scattering angle) and r is the direction along the lamellar stack.

The SAXS scattering curves were also fitted to a sum of power-law plus a Gaussian function (Blazek & Gilbert, 2011; Xu, Blennow, Li, Chen, & Liu, 2020) which obtained the full width at the half maximum (FWHM) of peak in the reciprocal space (W) for further discussions on SAXS the parameters:

$$I(q) = B + Pq^{-\alpha} + \frac{A\sqrt{\ln 4}}{W\sqrt{\pi/2}} \exp\left(-\frac{2 \ln 4(q - q_0)}{W^2}\right)$$

2.9. Fourier transform infrared-attenuated total reflectance (FTIR-ATR) spectroscopy

Spectra were acquired using a Bomem MB100 FTIR spectrometer (Bomem, Quebec, Canada) equipped with a Golden gate attenuated total reflectance (ATR) accessory. Prior to analysis, all the dry starch samples were equilibrated to equal ambient laboratory humidity. The spectra were collected at a resolution of 4 cm^{-1} and co-added for each sample. To obtain a background spectrum, the crystal was cleaned using a mixture of ethanol and water, and 128 co-added scans were recorded. The assumed line shape was Lorentzian with a half-width of 19 cm^{-1} and a resolution enhancement factor of 1.9. After baseline correction and deconvolution analysis using OMNIC software, IR absorbance values at 1022 and 1045 cm^{-1} were extracted from the spectra. It is worth noting that in the considered wavelength range (1065–870 cm^{-1}), the average penetration depth was estimated to be approximately 2 μm (Capron, Robert, Colonna, Brogly, & Planchot, 2007).

2.10. Scanning electron microscopy (SEM)

To analyze the morphology and morphology, the granules were fixed and sputter coated with gold, and imaged with a field emission scanning electron microscope (FE-SEM) (FEI Quanta 200) (Wang, et al., 2023).

2.11. Differential scanning calorimetry (DSC)

The gelatinization/melting temperatures for raw starches in excess distilled water (three times the weight of the starch equilibrated overnight) were determined by DSC (Mettler Toledo DSC1, Switzerland) in the range 20–180 °C at 5 °C/min in a high-pressure stainless steel DSC pan with gold-plated copper seal using an empty pan as the reference. The thermal transition temperatures and enthalpies of starches are reported as onset (T_o), peak (T_p), conclusion (T_c) and ΔH (J/g) as calculated by Stare Software version 9.1 (Mettler Toledo).

2.12. Statistical analysis

Analyses of all samples was carried out in duplicates. Data were expressed as a mean and standard deviation (SD) using analysis of variance (ANOVA) with Duncan's test. Statistical significance was defined at $p < 0.05$. The correlations were analyzed using Pearson correlation through the "cor" function and visualized using the R package "corrplot" (Wei & Simko, 2017).

3. Results and discussion

3.1. Apparent amylose content (AAC) and chain length distributions (CLDs) as analyzed by SEC and HPAEC-PAD

The AAC of the eight selected HAS and pure amylose types ranged from 34% to 97%, following the order of AOBs > Hylon VII > HAWS > NAFU60 > Gelose80 > NAFU50 > Gelose50 > HAPS (Table 1). The weight-based molecular size distribution profiles of the raw starches as analyzed by SEC (Fig. 1A) exhibited two regions: population I ($R_h > 66 \text{ nm}$) and population II ($R_h \leq 66 \text{ nm}$), in which are commonly recognized as the AP fraction and the AM fraction, respectively (Francisco Vilaplana & Robert G. Gilbert, 2010). The AM-only barley starch (AOBS), virtually devoid of AP and therefore consisting of almost pure AM, showed mainly one molecular population with peak at 30 nm in population II. HAPS displayed a major peak at 110 nm in the population I, and a smaller but broad peak at 30 nm in the population II. The other HASSs, containing a higher AAC, had peak maximum between 10 nm and 20 nm in population II, and a smaller AP peak ranging 100–110 nm in population I. For these samples except for AOBs (Table 1), the AP fraction could be divided into three levels: (I) starch with large AP molecules, HAPS (128 nm), (II) starches with medium AP molecules, NAFU50, NAFU60, Gelose

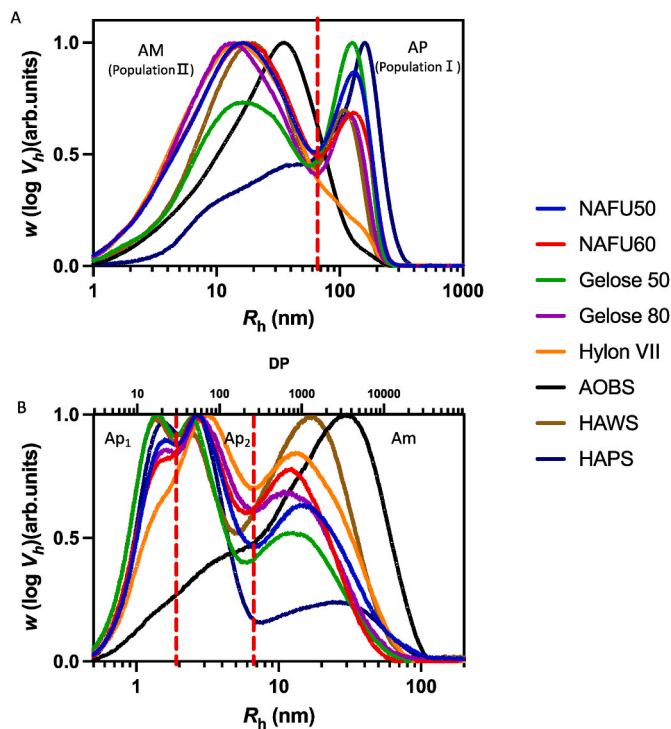


Fig. 1. SEC weight distributions of whole starch molecules, $w(\log V_{R_h})$, normalized to the maximum peak (A) and chain-length distributions (CLDs) of debranched samples (B).

(AM: R_h 0.6–66.5 nm; AP: R_h 66.5–1256 nm; Ap_{1-de}: DP 6–30; Ap_{2-de}: DP 30–220; Am_{de}: DP 220–10000)

(High amylose maize starches: NAFU50, NAFU60, Gelose 50, Gelose 80, Hylon VII; Amylose only barley starch: AOBS; High amylose wheat starch: HAWS; High amylose potato starch: HAPS).

50, Gelose 80, and HAWS (108–118 nm), and (III) starch with small AP molecules, Hylon VII (100 nm) based on their hydrodynamic radius (R_h). Based on the R_h of the AM fraction, the samples were also classified into three parts: (I) starches with large AM molecules, HAPS (13.9 nm) and AOBS (11.5 nm), (II) starches with medium AM molecules, HAWS (9.7 nm) and Gelose 50 (8.5 nm), and (III) starches with small AM molecules, Gelose 80, NAFU50, NAFU60, and Hylon VII (7.3–7.7 nm). The relative contents of the two populations were also measured based on the area under the curve and termed as RC_{na-AP} and RC_{na-AM} , respectively (Table 1). However, the data overestimated the RC_{na-AM} and underestimated the RC_{na-AP} , likely due to small AP molecules with a similar R_h to AM elute in the AM region (Vilaplana, Hasjim, & Gilbert, 2012). Hence, these two parameters are not further discussed.

The weighted-based CLD profiles of debranched starches as analyzed by SEC (Fig. 1B) exhibited three populations: population I (DP 6–30), population II (DP 31–200) and population III (DP > 200), which are commonly classified as short AP chains (Ap₁), long AP chains (Ap₂), and Am chains, respectively (Yu, et al., 2019). The peak maximum of the eight HASs was highly associated with botanical source, i.e., (I) the Ap₁ population dominated the potato starch HAPS, (II) the Ap₂ population dominated in the maize starches, Gelose 50, Gelose 80, NAFU50, NAFU60, and Hylon VII, and (III) the Am population dominated the Triticeae crops, AOBS and HAWS. It is worth mentioning that debranched AOBS also exhibited a minor fraction of short chains (DP < 100) in the Ap₁ and Ap₂ regions that are suggested to be the side chains of branched Am molecules (Fig. 1B). To verify whether AOBS contained AP molecules, the profiles of molecular size distribution and CLD of AOBS and Hylon VII was compared (Fig. S1B), and the results showed that debranching only slightly affected the molecular size distribution of AOBS but significantly decreased the molecular size of Hylon VII,

indicating AOBS can be classified as an AM-only starch and thus the removal of very few branches had consequently only minor effects of the R_h of starch molecules while Hylon VII is an AP-containing starch and thus debranching significantly decreased the molecular size of some AP molecules. It is worth noting that the few branches present in AM molecules of AOBS is attributed to the suppression of all starch branching enzymes in the AP biosynthesis pathway and the generation of “AM-like” materials (Zhong, Tai, et al., 2022). Furthermore, the debranching process of such materials using isoamylase and/or pullulanase is not entirely efficient, achieving up to 80% debranching (Hanashiro, 2015). The relative content and average chains of different fractions further substantiates the various molecular structures of these HASs (Table 1). Specifically, apart from AOBS, having extremely low contents in population I (6.9%) and population II (18.7%), all samples showed higher content of Ap₂ chains than Ap₁ chains (Table 1), which is typical for HAS (H. Li et al., 2019). In the AP-rich samples, the Ap₁ chains were predominant. For example, the Ap₁ content in diverse rice genotypes (AAC 1.5%–30.6%) was higher than 50%, and the Ap₂ content was between 18.3% and 26.5% (Zhong, Li et al., 2021). In the HAS starches (except for AOBS), HAPS showed the highest Ap₁ and Ap₂ contents, 37.4% and 40.4%, respectively; Hylon VII had the lowest Ap₁ content (16.6%), and the others had Ap₁ contents ranging 23.6–33.0%; HAWS had the lowest Ap₂ content (25.1%), and the others had Ap₂ contents ranging 33.2–35.8%. The average chain lengths (ACLs) of Ap₁ and Ap₂ fractions of AOBS were DP 14.9 and DP 89.9, respectively, and those of the other samples were lower, i.e., between DP 12.2–14.5 and DP 70.2–80.8, respectively. The ACLs of the Ap₁ chains of these HASs were similar to the AP-rich starches in rice with DP 13.0–14.6 (Zhong, Li et al., 2021), and the ACLs of the Ap₂ chains of these HAS samples, DP 68.0–89.9, were significantly higher than that of normal rice starches (DP 45.7–48.3). The relative content of population III, representing the AM fraction in AOBS was 74.3%, and that of other HASs ranged 22.2%–49.6%. Of the latter, Hylon VII and HAWS had the highest AC and HAPS had the lowest AC (Table 1). The higher apparent amylose content (AAC) in HAS and AOBS, as measured by iodine colorimetry, compared to the proportion of debranched chains > DP 200 (RC_{de-Am}), can be attributed to the longer amylopectin chains and the presence of “AM-like” materials, which have high affinity for iodine (H. Li et al., 2019). The ACLs of the AM chains in all samples ranged DP 870–DP 1600, and AOBS had the largest molecules and NAFU60 had the smallest ones. The AM CLD data were further fitted (Tao, Li, Yu, Gilbert, & Li, 2019; Yu, Tao, & Gilbert, 2018) (Tao et al., 2019; Yu, Tao et al., 2018), to account for the SEC band-broadening effects in the AM population. An example of this fitting process is shown in Fig. S1A. Subsequently, $\beta_{am,i}$ and $h_{am,i}$ values were calculated for the 3AM_i regions ($i = 1, 2, \text{ and } 3$, representing short, medium, and long AM chains, respectively). These values were used to reflect the ACLs and relative amounts of AM chains in these regions (Tao et al., 2019; Yu, Li et al., 2018; Yu, Tao et al., 2018), and are presented in Table 1. The h_{am} data indicated that the medium AM chains dominated all samples, and long AM chains were the second largest fraction in most samples except for NAFU60, Gelose 50, and Gelose 80. AOBS had the lowest β_{am} values in the three regions, reflecting that AOBS had the highest ACLs in all regions. HAPS had the highest β_{am} values in region 1 and region 2, showing that it had the lowest ACLs of short AM and medium AM chains. NAFU60 had the highest β_{am3} value, exhibiting that its ACL of long AM chains was the lowest among the different HASs.

The CLD profiles of samples as analyzed by HPAEC-PAD (Fig. S2 and Table 2) mainly reflect the variations in AP structure and AM short chain decorations. To clearly distinguish their differences, the chains were categorized into 4 subfractions: fa (DP 6–12), fb₁ (DP 13–24), fb₂ (DP 25–36) and fb₃ (DP > 36) (Bertoft, 2017), and their ACLs and relative contents (RCs) determined (Zhong, Liu, Qu, Blennow, et al., 2020). The data demonstrate that (I) HAWS and AOBS had the highest RC of short chains (DP 6–12) and higher amount of long chains (DP > 36); (II) NAFU50 and NAFU60 had more short and medium chains (DP 6–12 and

Table 2

Amylopectin molecular sub-chain structures of different HASs as deduced from HPAEC-PAD data.

Samples	Average chain lengths (ACLs) (DP)				Relative proportions (RC) (%)			
	fa	fb ₁	fb ₂	fb ₃	fa	fb ₁	fb ₂	fb ₃
NAFU50	10.5 ± 0.6 ^a	18.5 ± 0.0 ^c	29.5 ± 0.0 ^{de}	52.4 ± 0.4 ^a	8.7 ± 0.4 ^b	44.4 ± 0.9 ^a	22.8 ± 0.0 ^c	23.7 ± 1.3 ^d
NAFU60	10.5 ± 0.0 ^a	18.4 ± 0.0 ^c	29.4 ± 0.0 ^c	52.7 ± 0.3 ^a	9.0 ± 0.0 ^b	45.0 ± 0.3 ^a	22.8 ± 0.3 ^c	22.8 ± 0.1 ^d
Gelose 50	10.5 ± 0.0 ^a	18.6 ± 0.0 ^{ab}	29.8 ± 0.0 ^{abc}	48.4 ± 0.5 ^b	7.9 ± 0.2 ^c	36.7 ± 0.5 ^b	25.1 ± 0.1 ^b	30.0 ± 0.8 ^{abc}
Gelose 80	10.4 ± 0.1 ^a	18.6 ± 0.0 ^{ab}	29.8 ± 0.0 ^{abc}	48.6 ± 0.4 ^b	7.7 ± 0.3 ^c	35.3 ± 1.1 ^b	25.2 ± 0.2 ^b	31.4 ± 1.3 ^a
Hylon VII	10.5 ± 0.1 ^a	18.7 ± 0.0 ^a	29.9 ± 0.1 ^{ab}	48.5 ± 0.7 ^b	7.0 ± 0.1 ^c	35.9 ± 2.4 ^b	26.0 ± 0.2 ^b	30.9 ± 2.6 ^{ab}
AOBS	9.9 ± 0.0 ^b	18.6 ± 0.0 ^b	30.0 ± 0.0 ^a	48.4 ± 0.6 ^b	10.2 ± 0.2 ^a	34.3 ± 0.9 ^b	25.5 ± 0.3 ^b	29.6 ± 1.6 ^{abc}
HAWS	10.3 ± 0.0 ^a	18.4 ± 0.0 ^c	29.7 ± 0.0 ^{bc}	47.7 ± 0.6 ^b	10.7 ± 0.3 ^a	38.9 ± 0.3 ^b	23.6 ± 0.1 ^c	26.4 ± 0.7 ^{bcd}
HAPS	10.4 ± 0.1 ^a	18.6 ± 0.0 ^{ab}	29.7 ± 0.1 ^{cd}	51.0 ± 1.4 ^a	7.3 ± 0.4 ^c	38.6 ± 2.1 ^b	28.3 ± 0.9 ^a	25.6 ± 0.7 ^{cd}

All data are means ± standard deviation (n = 2). Values with different letters in the same column are significantly different at $p < 0.05$.

RC_x: relative amount of fraction X of debranched samples; ACL_x: average chain lengths (DP) of fraction X of debranched samples; fa: amylopectin chains with DP 6–12; fb₁: amylopectin chains with DP 13–24; fb₂: amylopectin chains with DP 25–36; fb₃: amylopectin chains with DP > 36.

12–24) and less long chains (DP > 24); (III) HAPS had the highest RC of DP 25–36; (IV) Gelose 50, 80 and Hylon VII had more long chains (DP > 24) and less short chains (DP < 24). Among all the samples, the variations in ACLs of the medium chains (DP 12–24) were insignificant, while a notable variation was found for short (DP 6–12) and long (DP > 36) chains. Overall, NAFU50 and NAFU60 showed less amount, but high ACL of long chains (DP > 36) while HAWS and AOBS showed high amount but low ACL of short chains (DP 6–12).

3.2. Degree of branching and helical structure

The degree of branching (Table 3) as deduced from ¹H NMR spectroscopy (Fig. S3) showed that the HASs ranged 1.4%–2.8%, in which Gelose 50 and Gelose 80 showed the highest degree of branching, with the values of 2.8% and 2.4%, respectively, and AOBS, NAFU60, and Hylon VII had the lowest values, ranging 1.4%–1.5%.

The relative double helical, single helical and amorphous contents (Table 3) analyzed by ¹³C NMR demonstrated that Gelose 50 and Gelose 80 had the lowest relative contents of the amorphous material,

amounting 55.5% and 53.0%, respectively, and NAFU50, NAFU60, HAWS, and AOBS, were mostly amorphous, with relative contents of 78.5%, 78.5%, 78.0%, and 68.5%, respectively. Among the eight HAS types, AOBS and HAWS, were single helical dominant, and AOBS had the highest percentage of single helices (16.0%). The other six types of starches were double helical dominant, and Gelose 50 and Gelose 80 had the highest relative contents of double helices, 31.0% and 32.5%, respectively. Three of them had extremely low content of single helices, 5.0% for NAFU50 and NAFU60, and 2.0% for HAPS. The other three types were also rich in single helical content, 13.8% in Hylon VII, 13.0% in Gelose 50, and 15.0% in Gelose 80, respectively.

3.3. Crystalline structure and lamellar structure

The crystalline polymorphs as deduced from WAXS data (Fig. 2) showed that all starches displayed a combination of B-type (at $2\theta = 17^\circ$, 22° , and 26°) and V_h-type (at $2\theta = 8^\circ$, 13° , 15° , and 20°) polymorphs, with a main peak at $2\theta = 20^\circ$ in AOBS and $2\theta = 17^\circ$ in other seven types of starches, indicating that AOBS was V_h-type dominant and the others

Table 3

Degree of branching, helical structure, crystalline structure, short range order, and lamellar structure of different HASs.

Sample	α -1,6/ α -1,4 ratio	Single helix (%)	Double helix (%)	Amorphous (%)	FTIR ratio (1045/ 1022 cm ⁻¹)	Crystallinity (%)	% V-type crystallinity	% B-type crystallinity	D (nm)	d _{ac} (nm)	d _a (nm)	d _c (nm)	q (nm ⁻¹)	W (a. u.) × 10 ⁻²
NAFU50	1.9 ± 0.1 ^c	5.0 ± 1.0 ^c	16.2 ± 0.6 ^{cd}	78.5 ± 0.5 ^a	0.7 ± 0.02 ^b	30.9 ± 2.0 ^a	3.7 ± 0.0 ^b	27.1 ± 2.0 ^a	8.9 ± 0.0 ^b	8.9 ± 0.0 ^b	1.9 ± 0.0 ^c	6.8 ± 0.1 ^b	0.71 ± 0.00 ^a	2.7 ± 0.1 ^{de}
NAFU60	1.5 ± 0.1 ^d	5.0 ± 0.0 ^c	16.3 ± 0.2 ^{cd}	78.5 ± 0.5 ^a	0.5 ± 0.03 ^c	21.8 ± 2.8 ^{bc}	3.0 ± 0.1 ^c	18.8 ± 2.7 ^{bc}	9.0 ± 0.1 ^b	8.9 ± 0.0 ^b	1.9 ± 0.0 ^c	7.0 ± 0.1 ^b	0.70 ± 0.00 ^a	3.0 ± 0.0 ^{de}
Gelose 50	2.8 ± 0.0 ^a	13.0 ± 0.0 ^{ab}	31.0 ± 1.0 ^{ab}	55.5 ± 0.6 ^c	0.5 ± 0.01 ^c	17.5 ± 0.0 ^{cd}	3.8 ± 0.0 ^b	13.7 ± 0.0 ^d	9.0 ± 0.0 ^b	9.1 ± 0.0 ^b	2.0 ± 0.0 ^{bc}	7.1 ± 0.0 ^b	0.69 ± 0.00 ^a	2.5 ± 0.0 ^e
Gelose 80	2.4 ± 0.0 ^b	15.0 ± 1.0 ^{ab}	32.5 ± 1.5 ^a	53.0 ± 1.0 ^c	0.6 ± 0.01 ^c	20.0 ± 2.3 ^{bc}	3.5 ± 0.5 ^{bc}	16.5 ± 1.8 ^{cd}	9.2 ± 0.1 ^b	9.2 ± 0.1 ^b	2.0 ± 0.0 ^{bc}	7.2 ± 0.1 ^b	0.68 ± 0.00 ^a	3.2 ± 0.1 ^{cd}
Hylon VII	1.5 ± 0.1 ^d	13.8 ± 0.8 ^{ab}	22.7 ± 1.4 ^{bc}	63.7 ± 2.3 ^b	0.5 ± 0.01 ^c	22.0 ± 0.7 ^{bc}	3.9 ± 0.2 ^b	18.0 ± 0.4 ^{bcd}	9.1 ± 0.1 ^b	9.1 ± 0.1 ^b	2.0 ± 0.0 ^{bc}	7.1 ± 0.0 ^b	0.69 ± 0.01 ^a	3.7 ± 0.1 ^c
AOBS	1.4 ± 0.1 ^d	16.0 ± 0.0 ^a	6.9 ± 0.4 ^d	76.7 ± 0.6 ^a	0.1 ± 0.05 ^e	13.8 ± 0.3 ^{de}	9.0 ± 0.0 ^a	4.8 ± 0.3 ^e	9.7 ± 0.2 ^a	9.7 ± 0.2 ^a	2.4 ± 0.1 ^a	7.3 ± 0.2 ^a	0.64 ± 0.01 ^b	5.3 ± 0.1 ^a
HAWS	1.9 ± 0.0 ^c	12.0 ± 0.0 ^b	10.0 ± 0.0 ^d	78.0 ± 0.0 ^a	0.4 ± 0.01 ^d	10.2 ± 0.2 ^c	1.8 ± 0.2 ^d	8.4 ± 0.5 ^e	9.2 ± 0.1 ^b	9.2 ± 0.1 ^b	1.9 ± 0.0 ^c	7.3 ± 0.0 ^b	0.68 ± 0.00 ^a	4.3 ± 0.4 ^b
HAPS	2.4 ± 0.1 ^b	2.0 ± 0.5 ^c	29.5 ± 4.5 ^{ab}	68.5 ± 2.5 ^b	0.9 ± 0.01 ^a	23.7 ± 0.9 ^b	1.0 ± 0.0 ^e	22.6 ± 0.8 ^{ab}	9.1 ± 0.0 ^b	9.1 ± 0.0 ^b	2.0 ± 0.0 ^b	7.0 ± 0.1 ^b	0.69 ± 0.00 ^a	2.5 ± 0.1 ^e

All data are means ± standard deviation (n = 2). Values with different letters in the same column are significantly different at $p < 0.05$.

Abbreviations are as follows: a.u., arbitrary unit; W(a.u.), the full width at half maximum (FWHM) of peak in reciprocal space from the SAXS data fitting; dac, da and dc, the thicknesses of total, amorphous, and crystalline lamellae, respectively.

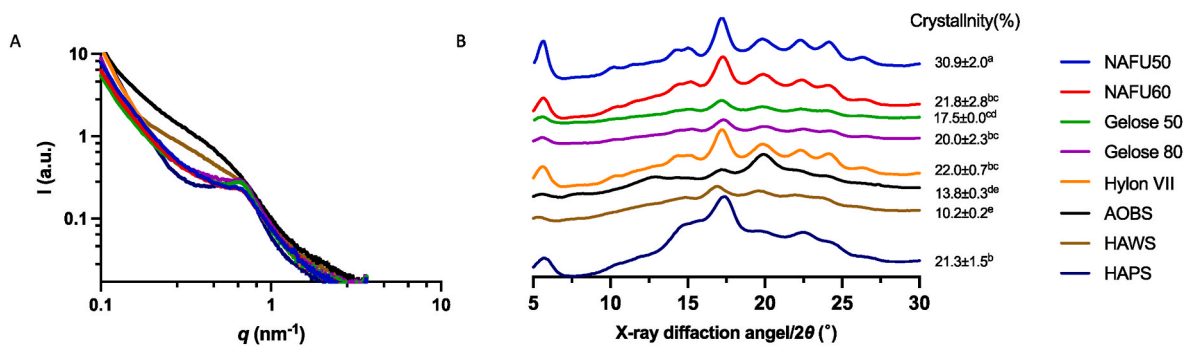


Fig. 2. 1D SAXS profiles (A), and WAXS spectra of different high amylose starches (B).

were mainly enriched in the B-type polymorph. This was further confirmed by the relative crystallinity data (Table 3), which ranged 10.2%–30.9%. The crystallinity of NAFU50 was the highest, with 30.9%, and that of AOBS and HAWS was the lowest, with 13.8% and 10.2%, respectively. All the other five types of starches had the crystallinity between 17.5% and 23.7%.

The SAXS profiles (Fig. 2) showed very different scattering patterns. HABS and HAWS showed extremely weak lamellar peak, while the other HASs presented observable approx. 9–10 nm lamellar peaks at 0.6–0.7 nm⁻¹, indicating HABS and HAWS had no, or very disordered, lamellar structure and the others had different alternating semi-crystalline lamellar structures. The lamellar related parameters (Table 3), analyzed as described in section 2.8, showed that, except for AOBS, the lamellar repeat distances of the HASs were between 8.9 and 9.2 nm. The thicknesses of the crystalline lamellae (d_c) and amorphous lamellae (d_a) ranged from 6.8 to 7.3 nm and 1.9–2.0 nm, respectively. This indicates that the HASs had similar lamellae thickness. The thickness of both the crystalline lamellae and the amorphous lamellae of AOBS were higher than the others, with the d_{ac} , d_a , and d_c calculated to 9.7 nm, 2.4 nm, and 7.3 nm, respectively. However, AOBS exhibited a broader SAXS peak as compared with the other HAS types (Fig. 2), indicating that AOBS had weak and disordered lamellar structure, rendering AOBS SAXS peak uncertain. The full width at half maximum of peak (FWHM) reflects the ordering of lamellar structure, and a higher FWHM value corresponds to lower lamellar structure ordering (H. Li, Dhital, Flanagan, et al., 2020; Xu et al., 2020). As expected, AOBS had the highest FWHM value 5.3, due to its lowest lamellar structural ordering. HAWS and Hylon VII showed relatively high FWHM values, 4.3 and 3.7 respectively, and disordered lamellar structure, corresponding to their relatively high AAC. Generally, FWHM showed a positive correlation with AAC ($r = 0.91$, Fig. 4), indicating that AAC is the primary parameter controlling the ordering of lamellar structure, due to the disrupting effect of AM on the lamellar structure by (I) co-crystallization with AP side-chains within the crystalline lamellae, (II) stacking within the amorphous lamellae, (III) forming AM tie-chains that pass through both the crystalline and amorphous lamellae, and (IV) affecting the alignment of AP double helices thereby preventing the formation of crystals (Koroteeva, Kiseleva, Srirath, et al., 2007; Zhong, Liu, Qu, Blennow, et al., 2020; Zhong, Tai, et al., 2022).

3.4. Surface order degree

The FTIR-ATR spectra of the HASs in the range of 800–1300 cm⁻¹, which corresponds to C–O and C–C stretching vibrations, provide insights into polymer conformation at the surface (~2 μm) of starch granules (Capron, et al., 2007). The presence of ordered and amorphous regions is indicated by the observed bands at 1045 cm⁻¹ and 1022 cm⁻¹, respectively (Van Soest, Tournois, de Wit, & Vliegthart, 1995). The ratio of 1045/1022 cm⁻¹ is commonly employed to evaluate the degree of surface order in starch. Among the various HAS samples, HAPS exhibited the highest degree of surface order (0.9), while HAWS and

AOBS demonstrated the lowest values of 0.4 and 0.1, respectively. HAMS displayed a comparable surface order degree, with NAFU 50 showing a relatively higher value of 0.7 (Table 3).

3.5. Granular morphology

The starch granular morphology as revealed by FE-SEM (Fig. 3) demonstrated very diverse granular shapes of HAS and AOBS granules, characterized by spherical, irregular elongated, and aggregated granules, in agreement with previous reports (H. Li, Dhital, Flanagan, et al., 2020). HAS granules are typically characterized by high level of agglomerated small granules embedded in a sheath (Glaring, Koch, & Blennow, 2006; Shaik et al., 2016). For NAFU50, NAFU60, Gelose50, Gelose80, and Hylon VII, the main morphologies found were spherical aggregation of small granular units, some of which presented elongated shapes. For the AOBS, the aggregated structures were very clear. HAWS had many sickle-shaped A-type granules (>10 μm diameter) (Fig. 3) as reported (Regina, et al., 2006). HAPS had regular, spherical, and smooth granular shapes (Fig. 3), rather similar to normal potato starch granules (Glaring et al., 2006; Jagadeesan, Govindaraju, & Mazumder, 2020).

3.6. Gelatinization properties

The effects of multi-scale structure of HASs on their gelatinization properties (Fig. S4, Table 4) showed that all HASs exhibited one major endotherm transition between 68.4 and 97.0 °C, attributed to the dissolution of their granular crystals (Liu, Yu, Xie, & Chen, 2006; Xu et al., 2020). HAWS had the lowest onset gelatinization temperature (T_o) with 53.5 °C, demonstrating its low crystalline, thermal resistance (Yuryev, et al., 2004). Most HASs, including HAPS, Gelose 50, Gelose 80, NAFU50, and NAFU60, exhibited onset gelatinization, T_o , between 64.5 and 71.4 °C. The T_o values of Hylon VII and AOBS were highest (83.6 °C and 87.8 °C, respectively), reflecting high thermal resistance. The gelatinization temperature range (the gap between conclusion temperature T_c and onset temperature T_o) reflects heterogeneity of crystalline structures in the granules (H. Li, Dhital, Flanagan, et al., 2020), and this heterogeneity decreased in the order HAWS > NAFU50, Gelose 50, Gelose 80 > HylonVII > AOBS, NAFU60 > HAPS (Fig. S4). The gelatinization enthalpy (ΔH) is said to be associated with the required thermal energy to mainly disrupt the granular crystalline structure (Singh, Singh, Kaur, Sodhi, & Gill, 2003), and the ΔH of dissolution was decreasing in the following order: Gelose50, Gelose 80, HAPS > NAFU50 > HAWS > HylonVII, NAFU60 > AOBS.

3.7. Multi-scale structural and functional relationships

Pearson correlation analysis was performed on the structural parameters described in Sections 3.1 to 3.3. This was done to identify relationships between the key molecular structures and their effects on short-range order (including surface order degree and helix content), lamellar and crystalline molecular packing (Fig. 4).

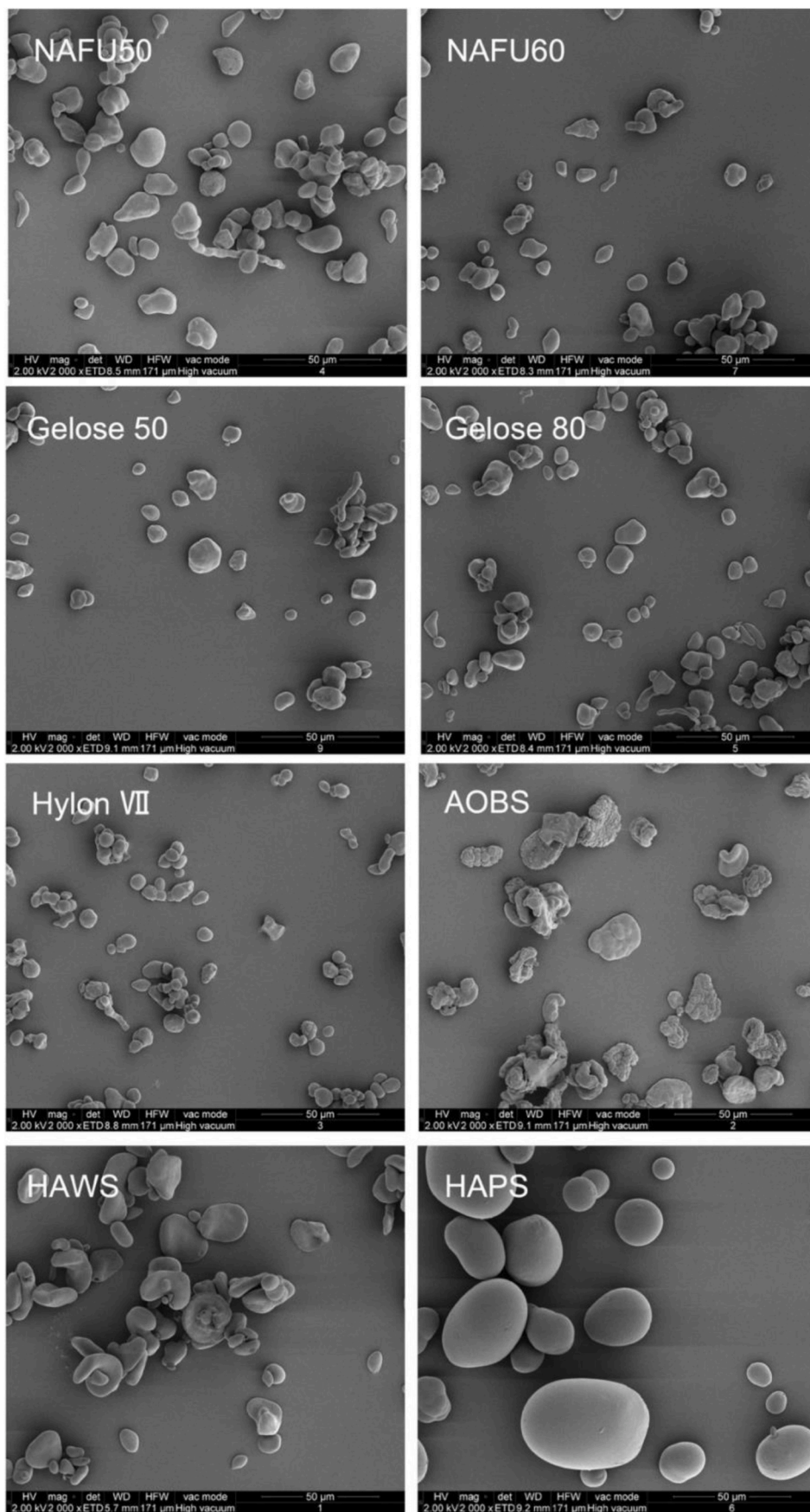


Fig. 3. FE-SEM micrographs of the HAS starches.

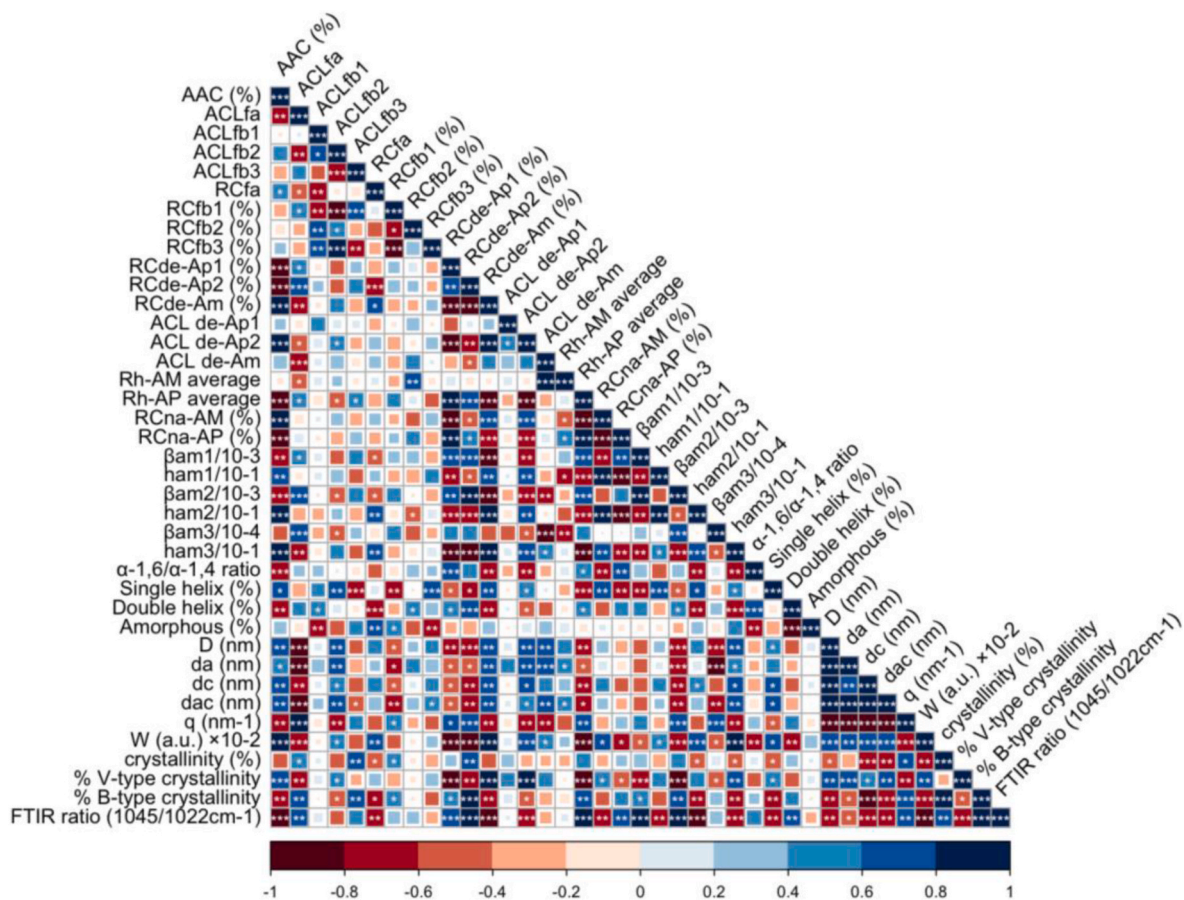


Fig. 4. Correlation analysis of the structural parameters of starches with different amylose content and different gene type (* $p < 0.05$, ** $p < 0.01$, *** $p < 0.001$).

Table 4

DSC parameters.

Samples	T_o ($^{\circ}\text{C}$)	T_p ($^{\circ}\text{C}$)	T_c ($^{\circ}\text{C}$)	ΔH (J/g)
NAFU50	70.1 ± 0.6^c	87.9 ± 1.0^b	109.3 ± 0.3^b	7.3 ± 0.7^b
NAFU60	71.4 ± 1.7^c	83.9 ± 0.3^b	93.9 ± 1.7^d	3.4 ± 0.8^{cd}
Gelose 50	64.9 ± 0.2^d	80.4 ± 0.2^b	108.6 ± 0.2^{bc}	11.5 ± 0.6^a
Gelose 80	66.0 ± 0.3^d	82.0 ± 0.2^b	105.6 ± 1.7^{bc}	10.9 ± 1.7^a
Hylon VII	83.6 ± 0.4^b	96.7 ± 0.6^a	108.9 ± 1.7^b	3.8 ± 0.2^{cd}
AOBS	87.8 ± 2.3^a	97.0 ± 1.4^a	105.9 ± 0.7^b	2.5 ± 0.6^d
HAWS	53.5 ± 1.1^e	68.4 ± 0.9^c	130.2 ± 0.8^a	5.8 ± 0.4^{bc}
HAPS	64.5 ± 0.2^d	69.8 ± 0.5^c	80.6 ± 0.3^c	11.0 ± 1.6^a

All data are means \pm standard deviation ($n = 2$). Values with different letters in the same column are significantly different at $p < 0.05$.

T_o : gelatinization onset temperature; T_p : gelatinization peak temperature; T_c : gelatinization conclusion temperature; ΔH : gelatinization enthalpy.

Degree of branching. Degree of branching (α -1,6/ α -1,4 ratio) (DB) was positively correlated with the content of Ap₁ chains (RC_{de-Ap1}), molecular size of AP molecules (Rh_{AP}), and the content of AP molecules (RC_{na-AM}), and negatively correlated with AC analyzed by iodine complexation (apparent amylose content, AAC), AC deduced from raw (RC_{na-AM}) and debranched SEC profiles (RC_{de-AM}), ACLs of Ap₂ chains (ACL_{de-Ap2}), relative amounts of medium (h_{am2}) and long (h_{am3}) AM chains. This mainly suggests that (I) AC is still the main factor correlated with the degree of branching of HASs, as reported (H. Li et al., 2019; Zhong, Tai, et al., 2022). While AC is an influential parameter, it is not the sole determining factor for the DB, a conclusion drawn from observing the significant differences in the branching degree of starches with comparable AAC and RC_{de-AM} values, such as NAFU60 with an AAC of 61% and branching degree of 1.5 and Gelose 80 with an AAC of 59% but a branching degree of 2.4, and this variance is likely attributed to higher

amount of AM₁ in Gelose 80, which may encompass "AM-like" molecules, as hinted by its short ACL_{de-AM} while large Rh_{na-AM}; (II) HASs with more medium and long AM chains are expected to have lower branching degree, implying that short AM chains possibly had more branches than medium and long AM chains. Furthermore, a higher degree of branching is more closely associated with an increased content of short AP chains (RC_{de-Ap1}); (III) HASs with higher degree of branching exhibited larger AP molecules, which is related to that branching increased the R_H of starch molecules (Castro, Ward, Gilbert, & Fitzgerald, 2005; Francisco Vilaplana & Robert G Gilbert, 2010).

Helical structure. The effect of AC on the content of double helical motifs was positively related to the degree of branching, i.e., higher AC resulted in lower double helix content, in agreement with the reporting effect of AM molecules on disrupting the packing the double helices (Koroteeva, Kiseleva, Krivandin, et al., 2007; Koroteeva, Kiseleva, Srirath, et al., 2007; Zhong, Liu, Qu, Blennow, et al., 2020). Moreover, the double helical content was positively correlated with degree of branching, ACLs of fb₁ chains (ACL_{fb1}), content of fb₂ chains (RC_{fb2}), content of Ap₁, Ap₂ (RC_{de-Ap1}, RC_{de-Ap2}), molecular size of AP molecules (Rh_{AP}), and negatively correlated to content of fa chains (RC_{fa}) and relative amounts of medium (h_{am2}) and long AM chains (h_{am3}). These data mainly implies mainly three considerations: Firstly, these parameters relate to so called connector chains (part of fb₁ chains and whole fb₂ chains) connected between long backbone chains and double helical segments according to the backbone model for starch (Bertoft, 2018; Zhong, Bertoft, Li, Blennow, & Liu, 2020) playing an important role on guiding the packing of double helices along the backbone, as suggested for a number of normal rice starch types (Zhong, Li et al., 2021). Secondly, decreasing the content of fa chains, which form the main component of the double helical segments (Bertoft, 2018; Zhong et al., 2020) promotes the packing and arrangement of a double helical,

lamellar structure, likely by decreasing the amounts of crystal defects (Koroteeva, Kiseleva, Sriroth, et al., 2007). Thirdly, less medium and/or long AM chains result in HAS with increased double helical content, which is an effect of that such AM chains, when present in the crystalline double-helical lamellae, prevent the formation of double helices (Zhong, Qu et al., 2022). As expected (Carciofi, et al., 2012; Obiro, Sinha Ray, & Emmambux, 2012), AC showed a positive correlation with the single helix content, due to the preferential folding of AM molecules to single helices (Putaux, et al., 2011). Furthermore, the content of single helices showed a negative correlation with β_{am1} and β_{am2} (lower value means longer AM chains in the region) but positive correlation to the amounts of chains in the Am1 and Am2 regions (h_{am1} and h_{am2}), indicating that short AM and medium AM chains were the main contributors of the single helical structure and that higher ACLs of these fractions resulted in higher single helical content. The content of amorphous material was not significantly correlated with AC, indicating that AC was not a vital molecular parameter for the amorphous region. Instead, the AP structure was more important, i.e., the relative content of the amorphous part showed positive correlation with the relative contents of fa and fb₁ chains (RC_{fa} and RC_{fb1}), and a negative correlation with the ACL of fb₁ (ACL_{fb1}), the relative content of fb₃ chains (RC_{fb3}), and degree of branching. This indicates that (I) AP molecules with low degree of branching had higher possibility to locate at the amorphous region, (II) AP molecules with more fa and fb₁ chains, less fb₃ chains, and lower ACLs of fb₁ chains are possibly mainly amorphous and not involved in the crystalline region, despite the higher content of helix-forming fa chains.

Lamellar structure. The thickness of the crystalline and amorphous lamellae was both positively correlated with AC parameters (especially for the ACL of long and medium AM chains), ACLs of fb₂ chains, ACLs of AM chains (ACL_{de-AM}), and single helix content, and negatively correlated with ACLs of fa chains (ACL_{fa}), the content of fb₁ chains (RC_{fb1}), molecular size of AP molecules (Rh_{de-AP}), β_{am2} , β_{am3} , and crystallinity. The correlation data confirms that AM is an important contributor for the lamellar structure of HASs as reported (Koroteeva, Kiseleva, Krivandin, et al., 2007; Koroteeva, Kiseleva, Sriroth, et al., 2007; Zhong, Tai, et al., 2022). We can now further elaborate that higher AC (especially more long AM chains) and longer AM chains (especially longer medium and long AM chains) result in HASs with thicker crystalline and amorphous lamellae. It has been suggested that long AM chains mainly orient within the amorphous lamellae (Koroteeva, Kiseleva, Krivandin, et al., 2007; Yuryev et al., 2004; Zhong, Liu, Qu, Blennow, et al., 2020) and branched AM molecules, so-called 'AM-like material', which are AM molecules suggested to be generated by SBE-suppressed mutants (Zhong, Qu et al., 2022), displace the function of AP molecules in which AM backbone chains stacked in the amorphous lamellae and their branches forms helical structures in the crystalline lamellae. This is well-supported by the existence of lamellar structure in the AM-only starch, AOBS, although AM resulted in a weak and disordered lamellae structure (Table 3). Based on this assumption, it is reasonable that long AM chains affects both amorphous and crystalline lamellae. Furthermore, the correlation analysis indicates that longer AP fb₂ chains contributed to thicker crystalline lamellae and amorphous lamellae, perhaps due to that these chains can possibly be double helix connector chains (Zhong et al., 2020; Zhong, Li et al., 2021) and located in both amorphous lamellae (as backbone chains) and crystalline lamellae (forming helical structures) (Bertoft, 2017). Thus longer chains resulted in thicker lamellar structures. A few studies reporting relationships between AC and lamellar structural parameters by using starches with a lower, but wider, range of AC (i.e., 0%–50%) has revealed no effects of AC on lamellar structure (Cardoso & Westfahl, 2010; Koroteeva, Kiseleva, Krivandin, et al., 2007; Koroteeva, Kiseleva, Sriroth, et al., 2007; Yuryev et al., 2004), which at first glance is inconsistent with our conclusion. However, data from starch systems with higher AM contents derived also from different genotypes with similar AC contents is here demonstrated to reveal clear effects on the lamellar structures. The data

show that the thickness of both the crystalline and the amorphous lamellae were positively correlated with the single helix content and negatively correlated with crystallinity suggesting that HASs with thicker crystalline lamellae and amorphous lamellae had less ordered crystalline structures. The FWHM, an indicator of lamellar structure ordering, where a lower value signifies higher lamellar ordering (Blazek et al., 2011; Xu et al., 2020), generally exhibited a positive correlation with the thicknesses of both crystalline and amorphous lamellar parameters, specifically da and dc. This suggests that HASs with thicker crystalline and amorphous lamellae tend to have a less ordered lamellar structure. In addition, the FWHM was also positively correlated with the content of single helices, and negatively correlated with the length of the fa chains, β_{am1} , β_{am2} , β_{am3} , degree of branching, and the content of double helices, mainly suggesting that (I) double helices stabilize the lamellar structure and single helices has a disordering effect on the lamellar structure, which is in agreement with the effect of AC on lamellar structure, and (II) longer AM chains resulted in more disordered lamellar structure, which is consistent with the negative correlation found between the single helix content and β_{am1} , β_{am2} , β_{am3} .

Crystalline structure. Total crystallinity (the sum of the B-, and V-type crystal contents) of HASs and the crystallinity of the B-type crystals were both positively correlated ACLs of the fa and fb₃ chains, and the content of fb₁ chains, and negatively correlated with the content of fa chains, the relative amounts of medium AM chains, and the content of single helices. This mainly demonstrates that (I) the B-type crystal polymorph is the main crystal type in HASs (Table 3), (II) the short branches, fa and fb₁ chains are important for crystalline structure ordering, again supporting that short fa chains form crystal defects, long fa chains and fb₃ chains build more perfect crystals, and long fb₁ chains function as connector chains as reported (Bertoft, 2017), and (III) the effect of medium AM chains, which are mainly located in the crystalline lamellae (Zhong, Liu, Qu, Blennow, et al., 2020), are mainly to disrupt crystalline structures likely by forming crystalline defects such as single helices in a double helical matrix. The content of the V-type crystalline polymorph showed an opposite correlation with structural parameters such as total crystallinity and B-type crystallinity, due to that AM is a main contributor to V-type crystals (H. Li et al., 2019; Obiro et al., 2012).

Granular surface structural order degree. Infrared spectroscopy has been suggested as a powerful tool for assessing short-range order in starch, supposed to be the presence of double helices. FTIR-ATR allows for the examination of the outer, approximately 2 μ m, surface layer of a starch granule (Sevenou, Hill, Farhat, & Mitchell, 2002), offering valuable insights into the degree of short-range order in this outer layer. Our data yielded the following key findings: (I) The FTIR wavenumber ratio 1045/1022 cm^{-1} shows a positive correlation with both the double helix content and B-type crystallinity. Furthermore, specific amylopectin structures, including ACL_{fa} , $RC_{de-AP1,2}$, and Rh_{AP} , which are contributors to double helices and B-type crystallinity discussed above, also displayed positive relationships with the degree of surface order. (II) Conversely, amylose had a negative impact on the surface order degree, aligning with its influence on double helix content and B-type crystallinity. Notably, the fine structure of amylose types encompassing average chain length and the relative amount of short (AM₁) and medium amylose chains (AM₂), significantly disrupts the degree of surface order. Longer and higher quantities of AM_{1,2} chains were associated with a lower degree of surface order. For instance, consider the HAS variant NAFU50, which exhibits a higher surface order degree compared to NAFU60, Gelose 50, and Gelose 80, despite having a similar RC_{de-Am} value. This difference can be attributed to NAFU50's shorter and lower content of AM_{1,2}, contributing to a more ordered surface structure.

Thermal properties. Correlation analysis between thermal properties and structural parameters of HASs (Fig. S5) mainly exhibited that the onset gelatinization and peak gelatinization temperatures (T_o and T_p , respectively), were positively correlated with AC, single helix content, and V-type crystalline content, and negatively correlated with the degree of branching, demonstrating that increasing AC resulted in higher

T_o and T_p , as reported previously (Jane, et al., 1999; Varavinit, Shobsngob, Varayanond, Chinachoti, & Naivikul, 2003) by enhancing the content of single helices and the associated V-type crystalline polymorph. Gelatinization enthalpy showed a positive correlation with the surface short-range order degree (1045/1022 cm^{-1} FTIR ratio), double helix content and degree of branching, and negative correlation with AC and full width at half maximum, indicating that degree of branching, molecular order (double helical and surface short-range order degree) structure and lamellar structural ordering were mainly responsible for the thermal energy consumption during HAS gelatinization, in agreement with the previous studies (Tian, et al., 2022; Varavinit et al., 2003). The positive correlation found between gelatinization enthalpy and $\beta_{\text{am}1}$ and $\beta_{\text{am}2}$ indicates that shorter AM_1 and AM_2 chains resulted in higher gelatinization enthalpy perhaps due to that shorter AM_1 and AM_2 chains more readily co-participate in the building of an ordered lamellar structure.

3.8. The classification and schemed multi-scale structural models of HASs

Irrespective of the AC, the thermal properties of the HASs and AOBs, starches were found in four groups (Fig. 5): (I) Gelose50 and Gelose80, having high gelatinization enthalpies (10.9–11.5 J/g) and low onset (64.9–66.0 °C) and peak (80.4–82.0 °C) gelatinization temperatures, (II) HAPS and HAWS, having medium to high gelatinization enthalpies (5.8–11.0 J/g) and extremely low onset (53.5–64.5 °C) and peak (68.4–69.8 °C) gelatinization temperatures, (III) NAFU 50 and NAFU60 having medium gelatinization enthalpies (3.4–7.3 J/g) and medium onset (70.1–71.4 °C) and peak (83.9–87.9 °C) gelatinization temperatures, (IV) Hylon VII and AOBs, having low gelatinization enthalpies (2.5–3.8 J/g) and high onset (83.6–87.8 °C) and peak (96.7–97.0 °C) gelatinization temperatures. It is clear that this classification is not significantly associated with AC and botanical source, as HAWS and AOBs had similar AC but very different thermal properties and the maize Hylon VII behaved differently compared with the maize NAFU series and maize Gelose series even though these were all SBEIIb-suppressed maize genotypes. In combination with the multi-scale structural and thermal data correlation analysis above, it is concluded that the degree of branching is a key structural parameter determining the thermal properties of HASs, i.e., HAS with higher degree of branching (Table 3), had higher gelatinization enthalpy and lower onset and peak gelatinization temperatures (Table 4). It is suggested that,

among HASs, the degree of branching in the AP and AM fractions collectively controls the gelatinization properties by affecting the RC of double helices (Fig. 4) which is the starch fraction requiring highest thermal energy to disrupt (Liu, et al., 2006; Xu et al., 2020).

The HASs can also be divided into two populations based on the structural ordering of granules related to botanical source. The first population was from triticeae crops, HAWS and AOBs, with the lowest crystallinity, the thickest crystalline lamellae, and highest FWHM of lamellar peak (Table 3), indicating their disordered crystalline and lamellar structure. The other six types of starches constituted another population, with more ordered crystalline and lamellar structure. This suggests that the structure of HASs from triticeae crops are less ordered than those from maize and potatoes, which has been suggested elsewhere comparing Gelose 80 and a HAWS mutant (H. Li, Dhital, Flanagan, et al., 2020). We provide new data suggesting that higher content of fa chains and higher amounts of medium and long AM chains in HAWS and AOBs were the main contributors of the low structural ordering of these granules, which prevented the formation of double helices (Fig. 4 and section 3.6) and instead formed single helix-dominating, V-type granules (Table 3). However, AOBs showed a higher content of V-type crystallinity (formed by single helices), which may be due to its longer amylose chains (AM_2 and AM_3) and less degree of branching.

4. Conclusion

The present study compares multi-scale structures and gelatinization behavior for eight types of HASs extracted from wheat, barley, maize, and potato. The relationships among parameters derived from molecular-, helical-, lamellar- and crystalline structures, and thermal properties was discussed. Correlation analysis showed that the molecular structural differences among the starches are the crucial factors impacting their higher levels of structure and gelatinization properties. For example, (I) shorter fa chains contributed to both thicker crystal and amorphous lamellar structures and more defects in the crystal structure (higher FWHM of lamellar peak and lower crystallinity); (II) the relative amounts and ACL of long amylose chains in the high-amylose starches were both positively correlated with the thickness of crystalline lamellae, V-type crystallinity and full width at half maximum of lamellar peak, and negatively correlated with degree of branching, the molecular order degree (double helices content and surface short range order degree), and B-type crystallinity, and (III) the degree of branching and the

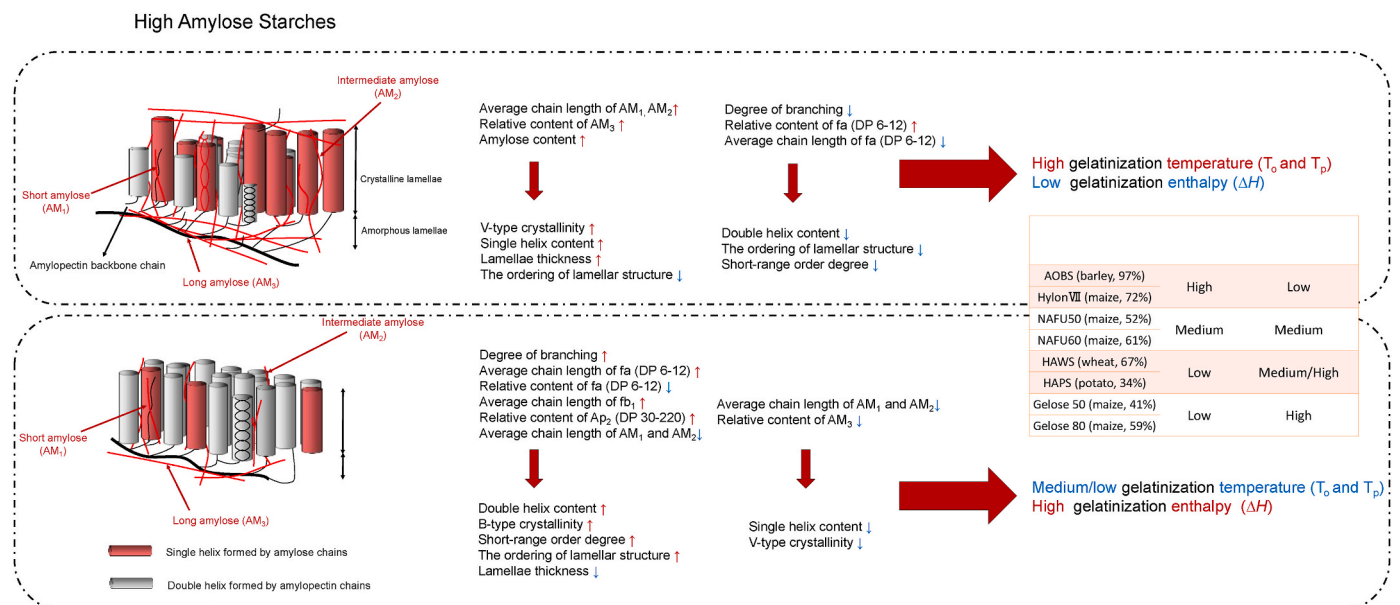


Fig. 5. Multi-level structure of high amylose starches and the thermal properties.

V-type crystallinity were the key structural parameters determining their gelatinization properties. Therefore, the structural parameters of the both the amylose and amylopectin component combine to influence the granular organization and application properties of HASs. The organization of the granular structure of these HASs was botanical source-related, but the gelatinization properties were not related to botanical source or amylose content. It is expected that the outcome of this study provides universal information for engineering and breeding of novel high amylose mutants from different crops and the application of high HASs in industry, e.g., bioplastics and resistant starch. Additionally, we are actively probing into the resistance mechanisms exhibited by diverse HAS starch granules, and those investigations are currently in progress.

Author statement

Yu Tian: Conceptualization, Investigation, Methodology, Software, Writing - Original Draft, Writing - Review & Editing.

Xingxun Liu: Methodology, Writing - Review & Editing.

Jacob Judas Kain Kirkensgaard: Investigation, Writing - Review & Editing.

Bekzod Khakimov: Investigation, Writing - Review & Editing.

Kasper Enemark-Rasmussen: Investigation, Writing - Review & Editing.

Kim Henrik Hebelstrup: Resources, Writing - Review & Editing.

Andreas Blennow: Conceptualization, Supervision, Funding acquisition, Writing - Review & Editing.

Yuyue Zhong: Conceptualization, Conceptualization, Supervision, Resources, Writing - Review & Editing.

Declaration of competing interest

The authors declare no competing financial interest.

Data availability

No data was used for the research described in the article.

Acknowledgments

Yu Tian gratefully acknowledges the support of the China Scholarship Council (CSC) funding for her PhD studies at the University of Copenhagen (UCPH), Denmark. Xingxun Liu acknowledges grants from the National Natural Science Foundation of China (32372476).

Appendix A. Supplementary data

Supplementary data to this article can be found online at <https://doi.org/10.1016/j.foodhyd.2023.109286>.

References

- Agama-Acevedo, E., Pacheco-Vargas, G., Bello-Pérez, L., & Alvarez-Ramirez, J. (2018). Effect of drying method and hydrothermal treatment of pregelatinized Hylon VII starch on resistant starch content. *Food Hydrocolloids*, *77*, 817–824.
- Bertoft, E. (2017). Understanding starch structure: Recent progress. *Agronomy*, *7*(3), 56.
- Bertoft, E. (2018). Analyzing starch molecular structure. In *Starch in food* (pp. 97–149).
- Blazek, J., & Gilbert, E. P. (2011). Application of small-angle X-ray and neutron scattering techniques to the characterisation of starch structure: A review. *Carbohydrate Polymers*, *85*(2), 281–293.
- Blennow, A., Bay-Smidt, A. M., Wischmann, B., Olsen, C. E., & Møller, B. L. (1998). The degree of starch phosphorylation is related to the chain length distribution of the neutral and the phosphorylated chains of amylopectin. *Carbohydrate Research*, *307* (1–2), 45–54.
- Blennow, A., Wischmann, B., Houborg, K., Ahmt, T., Jørgensen, K., Engelsen, S. B., et al. (2005). Structure function relationships of transgenic starches with engineered phosphate substitution and starch branching. *International Journal of Biological Macromolecules*, *36*(3), 159–168.
- Cai, C., Zhao, L., Huang, J., Chen, Y., & Wei, C. (2014). Morphology, structure and gelatinization properties of heterogeneous starch granules from high-amylose maize. *Carbohydrate Polymers*, *102*, 606–614.
- Capron, I., Robert, P., Colonna, P., Brogly, M., & Planchot, V. (2007). Starch in rubbery and glassy states by FTIR spectroscopy. *Carbohydrate Polymers*, *68*(2), 249–259.
- Carciofi, M., Blennow, A., Jensen, S. L., Shaik, S. S., Henriksen, A., Buléon, A., et al. (2012). Concerted suppression of all starch branching enzyme genes in barley produces amylose-only starch granules. *BMC Plant Biology*, *12*(1), 223.
- Cardoso, M. B., & Westfahl, H. (2010). On the lamellar width distributions of starch. *Carbohydrate Polymers*, *81*(1), 21–28.
- Castro, J. V., Ward, R. M., Gilbert, R. G., & Fitzgerald, M. A. (2005). Measurement of the molecular weight distribution of debranched starch. *Biomacromolecules*, *6*(4), 2260–2270.
- Glaring, M. A., Koch, C. B., & Blennow, A. (2006). Genotype-specific spatial distribution of starch molecules in the starch granule: A combined CLSM and SEM approach. *Biomacromolecules*, *7*(8), 2310–2320.
- Hanashiro, I. (2015). Fine structure of amylose. In Y. Nakamura (Ed.), *Starch: Metabolism and structure* (pp. 41–60). Tokyo: Springer Japan.
- Jagadeesan, S., Govindaraju, I., & Mazumder, N. (2020). An insight into the ultrastructural and physicochemical characterization of potato starch: A review. *American Journal of Potato Research*, *97*, 464–476.
- Jane, J., Chen, Y., Lee, L., McPherson, A., Wong, K., Radosavljevic, M., et al. (1999). Effects of amylopectin branch chain length and amylose content on the gelatinization and pasting properties of starch. *Cereal Chemistry*, *76*(5), 629–637.
- Khakimov, B., Mobaraki, N., Trimigno, A., Aru, V., & Engelsen, S. B. (2020). Signature Mapping (SigMa): An efficient approach for processing complex human urine 1H NMR metabolomics data. *Analytica Chimica Acta*, *1108*, 142–151.
- Koroteeva, D. A., Kiseleva, V. I., Krivandin, A. V., Shatalova, O. V., Blaszcak, W., Bertoft, E., et al. (2007). Structural and thermodynamic properties of rice starches with different genetic background: Part 2. Defectiveness of different supramolecular structures in starch granules. *International Journal of Biological Macromolecules*, *41* (5), 534–547.
- Koroteeva, D. A., Kiseleva, V. I., Sriroth, K., Piyachomkwan, K., Bertoft, E., Yuryev, P. V., et al. (2007). Structural and thermodynamic properties of rice starches with different genetic background: Part 1. Differentiation of amylopectin and amylose defects. *International Journal of Biological Macromolecules*, *41*(4), 391–403.
- Kuakpetoon, D., & Wang, Y.-J. (2007). Internal structure and physicochemical properties of corn starches as revealed by chemical surface gelatinization. *Carbohydrate Research*, *342*(15), 2253–2263.
- Kuang, Q., Xu, J., Liang, Y., Xie, F., Tian, F., Zhou, S., et al. (2017). Lamellar structure change of waxy corn starch during gelatinization by time-resolved synchrotron SAXS. *Food Hydrocolloids*, *62*, 43–48.
- Li, H., Dhital, S., Flanagan, B. M., Mata, J., Gilbert, E. P., & Gidley, M. J. (2020). High-amylose wheat and maize starches have distinctly different granule organization and annealing behaviour: A key role for chain mobility. *Food Hydrocolloids*, *105*, Article 105820.
- Li, C., Dhital, S., Gilbert, R. G., & Gidley, M. J. (2020). High-amylose wheat starch: Structural basis for water absorption and pasting properties. *Carbohydrate Polymers*, *245*, Article 116557.
- Li, R., Ding, L., Guo, K., Qu, J., Herburger, K., Persson, S., et al. (2023). The effects of different types of high-amylose maize starches on viscosity and digestion of acidified milk gels. *Food Chemistry*, *404*, Article 134525.
- Li, H., Gidley, M. J., & Dhital, S. (2019). High-amylose starches to bridge the "fiber gap": Development, structure, and nutritional functionality. *Comprehensive Reviews in Food Science and Food Safety*, *18*(2), 362–379.
- Li, H., Prakash, S., Nicholson, T. M., Fitzgerald, M. A., & Gilbert, R. G. (2016). The importance of amylose and amylopectin fine structure for textural properties of cooked rice grains. *Food Chemistry*, *196*, 702–711.
- Liu, H., Yu, L., Xie, F., & Chen, L. (2006). Gelatinization of cornstarch with different amylose/amylopectin content. *Carbohydrate Polymers*, *65*(3), 357–363.
- Nada, S. S., Zou, W., Li, C., & Gilbert, R. G. (2017). Parameterizing amylose chain-length distributions for biosynthesis-structure-property relations. *Analytical and Bioanalytical Chemistry*, *409*(29), 6813–6819.
- Obiro, W. C., Sinha Ray, S., & Emmambux, M. N. (2012). V-Amylose structural characteristics, methods of preparation, significance, and potential applications. *Food Reviews International*, *28*(4), 412–438.
- Putaux, J. L., Nishiyama, Y., Mazeau, K., Morin, M., Cardoso, M. B., & Chanzy, H. (2011). Helical conformation in crystalline inclusion complexes of V-amylose: A historical perspective. In *Macromolecular symposia* (Vol. 303, pp. 1–9). Wiley Online Library.
- Regina, A., Bird, A., Topping, D., Bowden, S., Freeman, J., Barsby, T., et al. (2006). High-amylose wheat generated by RNA interference improves indices of large-bowel health in rats. *Proceedings of the National Academy of Sciences*, *103*(10), 3546–3551.
- Sevenou, O., Hill, S. E., Farhat, I. A., & Mitchell, J. R. (2002). Organisation of the external region of the starch granule as determined by infrared spectroscopy. *International Journal of Biological Macromolecules*, *31*(1), 79–85.
- Singh, N., Singh, J., Kaur, L., Sodhi, N. S., & Gill, B. S. (2003). Morphological, thermal and rheological properties of starches from different botanical sources. *Food Chemistry*, *81*(2), 219–231.
- Tan, I., Flanagan, B. M., Halley, P. J., Whittaker, A. K., & Gidley, M. J. (2007). A method for estimating the nature and relative proportions of amorphous, single, and double-helical components in starch granules by ¹³C CP/MAS NMR. *Biomacromolecules*, *8* (3), 885–891.
- Tao, K., Li, C., Yu, W., Gilbert, R. G., & Li, E. (2019). How amylose molecular fine structure of rice starch affects functional properties. *Carbohydrate Polymers*, *204*, 24–31.
- Tian, Y., Qu, J., Zhou, Q., Ding, L., Cui, Y., Blennow, A., et al. (2022). High pressure/temperature pasting and gelling of starch related to multilevel structure-analyzed with RVA 4800. *Carbohydrate Polymers*, *295*, Article 119858.

- Tian, Y., Wang, Y., Zhong, Y., Møller, M. S., Westh, P., Svensson, B., et al. (2023). Interfacial catalysis during amylolytic degradation of starch granules: Current understanding and kinetic approaches. *Molecules*, 28(9), 3799.
- Van Soest, J. J., Tournois, H., de Wit, D., & Vliegthart, J. F. (1995). Short-range structure in (partially) crystalline potato starch determined with attenuated total reflectance Fourier-transform IR spectroscopy. *Carbohydrate Research*, 279, 201–214.
- Varavinit, S., Shobsngob, S., Varayanond, W., Chinachoti, P., & Naivikul, O. (2003). Effect of amylose content on gelatinization, retrogradation and pasting properties of flours from different cultivars of Thai rice. *Starch Staerke*, 55(9), 410–415.
- Vilaplana, F., & Gilbert, R. G. (2010a). Characterization of branched polysaccharides using multiple-detection size separation techniques. *Journal of Separation Science*, 33(22), 3537–3554.
- Vilaplana, F., & Gilbert, R. G. (2010b). Two-dimensional size/branch length distributions of a branched polymer. *Macromolecules*, 43(17), 7321–7329.
- Vilaplana, F., Hasjim, J., & Gilbert, R. G. (2012). Amylose content in starches: Toward optimal definition and validating experimental methods. *Carbohydrate Polymers*, 88(1), 103–111.
- Wang, Y., Tian, Y., Christensen, S. J., Blennow, A., Svensson, B., & Møller, M. S. (2023). An enzymatic approach to quantify branching on the surface of starch granules by interfacial catalysis. *Food Hydrocolloids*, Article 109162.
- Wei, T., & Simko, V. (2017). R package “corrplot”: Visualization of a correlation matrix. In *Vienna Version 0.84*.
- Wootton, M., & Bamunuarachchi, A. (1979). Application of differential scanning calorimetry to starch gelatinization. I. Commercial native and modified starches. *Starch Staerke*, 31(6), 201–204.
- Xu, J., Blennow, A., Li, X., Chen, L., & Liu, X. (2020). Gelatinization dynamics of starch in dependence of its lamellar structure, crystalline polymorphs and amylose content. *Carbohydrate Polymers*, 229, Article 115481.
- Yu, W., Li, H., Zou, W., Tao, K., Zhu, J., & Gilbert, R. G. (2019). Using starch molecular fine structure to understand biosynthesis-structure-property relations. *Trends in Food Science & Technology*, 86, 530–536.
- Yu, W., Tao, K., & Gilbert, R. G. (2018). Improved methodology for analyzing relations between starch digestion kinetics and molecular structure. *Food Chemistry*, 264, 284–292.
- Yuryev, V. P., Krivandin, A. V., Kiseleva, V. I., Wasserman, L. A., Genkina, N. K., Fornal, J., et al. (2004). Structural parameters of amylopectin clusters and semi-crystalline growth rings in wheat starches with different amylose content. *Carbohydrate Research*, 339(16), 2683–2691.
- Zhong, Y., Bertoft, E., Li, Z., Blennow, A., & Liu, X. (2020a). Amylopectin starch granule lamellar structure as deduced from unit chain length data. *Food Hydrocolloids*, 108, Article 106053.
- Zhong, Y., Herburger, K., Kirkensgaard, J. J. K., Khakimov, B., Hansen, A. R., & Blennow, A. (2021a). Sequential maltogenic α -amylase and branching enzyme treatment to modify granular corn starch. *Food Hydrocolloids*, Article 106904.
- Zhong, Y., Li, Z., Qu, J., Bertoft, E., Li, M., Zhu, F., et al. (2021b). Relationship between molecular structure and lamellar and crystalline structure of rice starch. *Carbohydrate Polymers*, 258, Article 117616.
- Zhong, Y., Liu, L., Qu, J., Blennow, A., Hansen, A. R., Wu, Y., et al. (2020b). Amylose content and specific fine structures affect lamellar structure and digestibility of maize starches. *Food Hydrocolloids*, 108, Article 105994.
- Zhong, Y., Liu, L., Qu, J., Li, S., Blennow, A., Seytahmetovna, S. A., et al. (2020c). The relationship between the expression pattern of starch biosynthesis enzymes and molecular structure of high amylose maize starch. *Carbohydrate Polymers*, 247, Article 116681.
- Zhong, Y., Qu, J. Z., Liu, X., Ding, L., Liu, Y., Bertoft, E., et al. (2022a). Different genetic strategies to generate high amylose starch mutants by engineering the starch biosynthetic pathways. *Carbohydrate Polymers*, Article 119327.
- Zhong, Y., Tai, L., Blennow, A., Ding, L., Herburger, K., Qu, J., et al. (2022b). High-amylose starch: Structure, functionality and applications. *Critical Reviews in Food Science and Nutrition*, 1–23.